Control of assembly size of poly (methacrylic acid)-grafted fullerenes in aqueous solution

doi: https://doi.org/10.1007/s10965-018-1575-6

Control of Assembly Size of Poly (Methacrylic Acid)-*grafted* Fullerenes in Aqueous Solution

Emiko Mouri, Sanami Moroi

Department of Applied Chemistry, Faculty of Engineering, Kyushu Institute of Technology,
1-1 Sensui, Tobata, Kitakyushu, Fukuoka 804-8550, Japan

*To whom correspondence should be addressed.
e-mail: mouri@che.kyutech.ac.jp, Tel & Fax: +81-93-884-3335

Key words: polymer-grafted fullerene, micelle, poly(methacrylic acid), aqueous solution, amphiphilic polymer

Abstract

We synthesized poly(methacrylic acid)-grafted fullerenes (PMA-C_{60}) with different PMA molecular weights and investigated the assembly size formed by PMA-C_{60} in aqueous solution. The molecular weight of PMA strongly affects the assembly size: PMA-C_{60} with a larger molecular weight forms micelles with 20 nm diameters while PMA-C_{60} with a smaller molecular weight forms monodisperse assemblies with 200 nm hydrodynamic diameters. We succeeded in converting the large monodisperse assembly into micelles by adding either ionic species or ethanol. This result provides insight into controlling the assembly size of fullerene-containing assemblies.

Introduction

Fullerene (C_{60}) is one of the most attractive materials in nanomaterial science because of its specific shape and versatile characteristics, including semiconduction, high thermal stability, high refractive index, high heat conductivity, and radical trapping properties[1,2]. One promising application for polymer-grafted fullerene is in organic solar cells[3,4] because of the high potential of fullerene to act as an electron acceptor. On the other hand, fullerene is reported to be effective in both medical and cosmetic applications[5–8]. For example, it is a promising medical candidate for the treatment of cancer[5,6], HIV[5,7], and Alzheimer's disease[5]. Important

issues affecting these applications of fullerene in material and biological sciences include the low solubility or miscibility of fullerene in general solvents or polymer matrixes. In applications such as drug delivery in particular, fullerenes must be dispersed in an aqueous solution. In order to achieve this, fullerenes are usually modified using polar groups or hydrophilic polymers[9–12]. It is imperative to ascertain the size effect of fullerene-containing materials on the human body as well as the solubility of these materials in water to establish their in vivo application. Specifically, the size effect on the drug effectiveness and toxicity in drug delivery systems (DDS) cannot be ignored in the range of a few nanometers to the order of submicron, as DDS drugs that are typically fabricated are in the range of 10 nm to 400 nm.

From the late 1990s to the present, many types of polymer-grafted fullerenes with a relatively monodisperse nature have been synthesized[11]. However, in some cases, the size of the assemblies exceeds 100 nm in diameter while micelles of a few nm in size are obtained in a similar system[13–26]. The size of these assemblies were found to exceed 100 nm in poly(ethylene oxide)[14], poly(acrylic acid)[15–18], poly(methacrylic acid)[19,20], and poly(*N*-isopropyl acrylamide)[24], while micelles with 3–5 nm hydrodynamic radii were observed in systems containing poly[2-(dimethylamino)-ethyl methacrylate][21–23]. An assembly exceeding 100 nm in size is a fairly large spherical micelle, considering the molecular weights of the components and the types of of hierarchical structures expected in the inner structures of these large assemblies[14–20].

At this stage, however, we do not have established criteria for the fabrication of fullerene-containing assemblies of desired sizes. The molecular weight dependence on the association behavior has not been reported in previous studies; this also makes it difficult to understand the association behavior systematically. Thus, we must understand the association behavior of a polymer-grafted fullerene system in order to control the assembly size since the association behavior of polymer-grafted fullerene is somewhat different when compared with conventional amphiphilic polymer systems.

Recently, we reported that poly(methyl methacrylate)-grafted fullerene forms a monodisperse assembly with a sub-micrometer diameter in acetonitrile[25]. In this case, the assembly size is much larger than that of a micelle size and appears to possess a hierarchical structure with micelles as building blocks. We also reported on the association behavior of poly(*N*-vinylpyrrolidone) (PVP)-grafted fullerenes[26]. PVP is non-toxic and water soluble and is widely used as a dispersant in the medical and cosmetic industry. In this system, PVP-grafted fullerenes form micelles in an aqueous solution with a hydrodynamic diameter of 20 to 30 nm. We observed a gradual increase in micelle size by adding free fullerenes up to ca. 30 nm; however a drastic increase in size 200 nm size assemblies was observed. From these studies, we suggested that the association behavior of these systems is not continuous but is instead characterized by the two different assembly structures, i.e., by the micelle and large assembly. If

the two different stable (or quasi-stable) states exist in a polymer-grafted fullerene system, then the general trend in the association behavior of the polymer-grafted fullerene system would be more complicated than that for typical amphiphiles; as such, it should be uniquely understood.

In this paper, we studied another type of polymer-grafted fullerene system, namely, poly(methacrylic acid) (PMA)-grafted fullerene, in order to elucidate the factors controlling the assembly size. PMA is a representative water-soluble polymer and is suitable for use in bio-materials[27]. It was found that PMA-C_{60} with a high molecular weight forms micelles 20 nm in diameter, while PMA-C_{60} with a low molecular weight forms a monodisperse assembly 200 nm in diameter. The large monodisperse assembly can be transformed into micelles by adding ionic species or ethanol. By demonstrating the controlling factor of the assembly size, we revealed the controlling factors and the underlying principles of the association behavior in polymer-grafted fullerene systems.

Experimental Section

Synthesis of PMA-Grafted Fullerene

To synthesize PMA-grafted fullerene, poly(*t*-butyl methacrylate) (P*t*BMA) homopolymer was first synthesized by iniferter polymerization. In a test tube, freshly distilled

*t*BMA monomer (Wako Pure Chemical Industries, Ltd., Osaka, Japan) and photoiniferter benzyl dithiocarbamate (BDDC) were mixed in dioxane (Kanto Chemical Co., Inc., Tokyo, Japan). BDDC was synthesized as previously described[26]. A typical feed of a few milliliters of dry *t*BMA and 45 mg BDDC in 3 ml dioxane was used, as shown in Table 1S. The mixture was carefully degassed using four or five freeze–pump–thaw cycles, followed by exposure to 3–5 h of UV irradiation using high-pressure mercury lamps (SX-UI500HQ and BA-H500; USIO Inc., Tokyo, Japan). After the reaction, P*t*BMA was re-precipitated using a methanol/water (90/10) mixture. The obtained polymer samples were characterized by ^{1}H-NMR spectroscopy (Avance-400; Brucker, Illinois, USA) and GPC. The GPC system was equipped with a column oven (CTO-10A/10AC; Shimadzu, Kyoto, Japan) and a refractive index detector (RI153; Jasco Corp., Tokyo, Japan).

In the second step, a reaction between P*t*BMA and fullerene (Fullerene, nanom purple st 98%; Frontier Carbon, Fukuoka, Japan) was conducted in dichlorobenzene. The fullerene feed was three times larger than that of P*t*BMA. The mixture of P*t*BMA and fullerene (1:3 molar ratio) in dichlorobenzene was degassed, placed under a N_2 atmosphere, and then subjected to 12 h of UV irradiation. The representative feeds for the samples are summarized in Table 2S. This reaction was carried out several times to obtain a reasonable amount of P*t*BMA sample. The reactant was precipitated in methanol and the precipitate was re-dispersed

in ethanol. The ethanol dispersion was centrifuged to form a precipitate of free fullerene, and the supernatant was evaporated to obtain the solid sample.

P*t*BMA-C_{60} (0.1 g) was then subjected to hydrolysis in 25 ml of 1,4-dioxane with 0.5 ml HCl refluxing at 80 ºC for 24 h. After the reaction, the reactant was poured into hexane to precipitate PMA-C_{60}. The obtained PMA-C_{60} was further purified by dialysis against water to remove non-fullerene-capped PMA. The inclusion of the fullerene moiety was confirmed by IR measurement (JIR-5500, Jasco Corp., Tokyo, Japan).

Size Estimation of the Self-Assemblies of PMA-C_{60}

In order to estimate how PMA-C_{60} forms an assembly in water, the surface tension of the PMA-C_{60} solution was measured at 22ºC in the range of 5.0×10^{-4} mM to 5.0×10^{-2} mM. The surface tension was measured with a CBVP-A3 (Kyowa, Tokyo, Japan).

The PMA-C_{60} samples were dissolved in Milli-Q water to perform dynamic light scattering (DLS) measurements. DLS measurements were performed using a DLS-7000 (Otsuka Electronics Co., Ltd., Hirakata, Japan) with a He–Ne laser (632.8 nm wavelength) at scattering angles of 75º, 90º, 105º, and 120º at 25 ºC. We obtained the time correlation function, $g^2(\tau)$, of the measured scattered intensity as defined by the following equation:

$$g^2(\tau) = \frac{\langle I(t)\, I(t+\tau)\rangle}{\langle I(t)\rangle^2}$$

where $I(t)$ is the scattered intensity at time t, and τ is the delay time. The time correlation of the scattering intensities is calculated at every τ. τ is the time difference between two arbitrary correlated data points. The time correlation function of the scattered amplitude, $g^1(\tau)$, is related to $g^2(\tau)$ by the following equation:

$$g^2(\tau) - 1 = \beta|g^1(\tau)|^2$$

where β is the coherent factor. Data analysis was carried out by curve fitting of $(g^2\text{-}1)^{1/2}$ to the exponential function $\beta^{1/2} \exp(-\Gamma\tau)$ as $g^1(\tau) = \exp(-\Gamma\tau)$. In this process, the decay rate Γ and coherent factor β are the fitting parameters. When the single exponential model could not reproduce the data, we introduced a double exponential model, $(g^2\text{-}1)^{1/2} = \phi(\beta^{1/2} \exp(-\Gamma_1\tau)) + (1 - \phi)(\beta^{1/2} \exp(-\Gamma_2\tau))$, where ϕ is a fraction of the first component. Maquardt analysis was also performed in addition to the exponential fitting.

By changing the scattering angle from 75° to 120°, a decay constant (Γ) vs. scattering vector (q^2) plot was made. The scattering vector is defined as $q = 4\pi n \sin\theta/\lambda$, where n is the refractive index, θ is the scattering angle, and λ is the laser wavelength. Using the linear relationship between Γ and q^2, we confirmed our observation of the lateral diffusion mode. The diffusion coefficient, D, was determined from the slope of the plot and converted into hydrodynamic radii using the Stokes–Einstein equation, $D = k_BT/3\pi\eta D_h$ (where D is the diffusion coefficient, T is the absolute temperature, η is the viscosity, and D_h hydrodynamic

diameter). Maquardt analysis was also applied to the DLS data. The values of the diffractive index and viscosity were 1.3329 and 0.8902 mPa・s, respectively, for the aqueous solutions. These values for the binary solvents were estimated from literature as described in the supporting information (Table 6S and Table 7S). TEM observation of the assembly was carried out with an H-9000NAR (Hitachi, Tokyo, Japan) and for comparison with the results obtained from the scattering and imaging methods.

Result and Discussion

Characterization of PMA-C_{60}

We synthesized three samples of P*t*BMA-grafted C_{60} with different molecular weights of P*t*BMA. The synthesized P*t*BMA has a number-average molecular weight ranging from 3,000 to 113,000, as shown in **Table 1**. Here, the sample code is based on the molecular weight of P*t*BMA. We confirmed the characteristics of the obtained samples by ^{1}H NMR spectroscopy [^{1}H NMR for P*t*BMA: δ: 0.97–1.18 (m, CH_2), 1.38–1.46 (m, $C(CH_3)_3$), 1.75–1.88 (m, CH_3) ppm; Figure 1S], and GPC. After the reaction with fullerene, the samples underwent hydrolysis to produce PMA-C_{60}. The obtained PMA samples were characterized by ^{1}H NMR spectroscopy as shown in Figure 2S. The completion of hydrolysis was confirmed by the disappearance of the peaks at 1.44 ppm based on the *t*-butyl groups [^{1}H NMR for PMA-C_{60}: δ: 1.05–1.24 (m, CH_2),

1.84–2.05 (m, CH_3) ppm]. Here, the sample codes following hydrolysis were changed from P*t*BMA*x*k-C_{60} to PMA*y*k-C_{60} on the basis of the re-calculated molecular weights of PMA. The incorporation of fullerene was confirmed by IR spectroscopy (Figure 3S). The specific peaks derived from fullerene at 527, 576, 1182, and 1429 cm^{-1} overlapped with those from the polymer component; however, the rather weak peak at 2325 cm^{-1} resulting from fullerene was confirmed for the P(*t*BMA)-grafted fullerene.

Association behavior of PMA-C_{60} in Water

Figure 1 shows the surface tension change with PMA-C_{60} concentrations measured at 22 ºC. The two samples of PMA14k-C_{60} and PMA45k-C_{60} show almost the same tendency in their surface tension–concentration relationships. **Figure 1** indicates that the critical micelle concentration (cmc) for PMA-C_{60} was around 10^{-5} M to 10^{-4} M. From this result, DLS measurements were carried at ca. 0.1 mM for all samples. The surface tension decrease was observed at a much lower concentration range compared with the PMA homopolymer system[28]; this could be attributed to the hydrophobic fullerene moiety.

We estimated by DLS the assembly size formed by PMA-C_{60} in water. In **Figure 2**, the time-correlation functions at a scattering angle of 90° are shown as representative data. The time-correlation function shows a difference in decay depending on the samples. Among the

data for the four samples, a slow decay of the exponential curve was observed for PMA2k-C_{60} and PMA14k-C_{60}; this suggests the formation of a large assembly in the PMA2k-C_{60} and PMA14k-C_{60} samples. We estimated the decay constant, Γ, for each time-correlation function by fitting with an exponential function in the form of $\exp(-\Gamma\tau)$, and subsequently plotted Γ against q^2, as shown in **Figure 3**. The time-correlation functions were well-fitted with a single exponential function for PMA2k-C_{60} and PMA14k-C_{60}, and with a double exponential function for PMA45k-C_{60} and PMA68k-C_{60}. One of the exponential functions with a fast decay is attributed to the formation of micelles and the other with a slow decay to larger assemblies. In **Table 2**, the assembly sizes obtained by the fittings are summarized. **Figure 4** indicates the relationship between the assembly size and grafted PMA molecular weight. The samples with a low molecular weight, i.e., PMA2k-C_{60} and PMA14k-C_{60}, show an assembly size of ca. 200 nm, which is much larger than a reasonable micelle size. The large assembly with 200 nm diameter demonstrated a rather monodisperse nature, which means that the large assembly is not a typical aggregate. For samples with a larger M_n of PMA, i.e., PMA45k-C_{60} and PMA68k-C_{60}, smaller assemblies were observed, ca. 20 nm in diameter, in addition to larger assemblies over 100 nm in hydrodynamic diameter. The latter assemblies comprised as little as 0.03% in a number-based fraction, as shown in **Figure 4**. The assemblies with 20–30 nm diameters are attributed to the presence of micelles.

We observed a large difference in the assembly sizes between the samples, which is not typical of conventional amphiphilic polymers with similar molecular weights. For example, a relevant amphiphilic copolymer system containing a PMA moiety was systematically studied by Munk et al. as polystyrene-*b*-poly(methacrylic aid) micelle solutions[29]. They showed the micelle radius of gyration in the range of 11 to 40 nm depending on the molecular weight of the polymer, which ranged from 30,000 to 180,000. It was found that most of the samples were of similar size. Eisenberg et al. systematically studied polystyrene-*b*-poly(acrylic acid) micelle solutions, a system similar to that examined in the present study. They showed that the micelle radius of gyration is proportional to $N_{PANa}^{3/5}N_{PS}^{4/25}$ (where N is the degree of polymerization) and that the size monotonically increased with the degree of polymerization[30,31]. Burguière et al. also reported on polystyrene-*b*-poly(acrylic aid) solutions and showed that the micelle radius is in the range of 25 to 35 nm for molecular weights ranging from 4,000 to 17,000 g/mol[31]. These data indicate that the usual size of the micelle radius is a few tens of nm over a similar molecular weight range and shows a monotonic increase with the molecular weight, which was not observed in the fullerene-grafted PMA system.

We next confirmed the assembly size by TEM. **Figure 5** shows TEM images for PMA14k-C_{60} and PMA45k-C_{60}. The TEM image for PMA14k-C_{60} shows monodisperse spherical assemblies with 200 nm diameters, which agree with the large components that were

estimated in the DLS analysis. On the other hand, the TEM image for PMA45k-C_{60} shows spherical assemblies with 20 nm diameters, which is also consistent with the DLS data and also suggests micelle formation. The monodispersed nature of this assembly ca. 200 nm in diameter suggests that this is not a usual aggregate, but rather an assembly that with an ordered structure. The large spherical assembly was also observed in our previous study of the PMMA-C_{60} system[25]. The PMMA-C_{60} sample showed that the large assembly that was present was composed of micelles, and that the surface of the large assembly was raspberry-like in appearance. By comparing the two systems, PMMA-C_{60} and PMA-C_{60}, we can see that the assembly of PMA-C_{60} has a smooth surface, which suggests that the inner structure of the large assembly differs between the two systems. Candidates for the composition of the inner structure are vesicles rather than large compound micelles (LCMs)[33,34]. LCMs are hierarchical assemblies of micelles, which were observed for the PMMA-C_{60} system in both our study[25] and other studies[15,16,20].

Effects of Ion Concentration on the Large Assembly

In the former section, we describe how the molecular weight of PMA affects the assembly size. Only large aggregates ca. 200 nm in diameter are obtained for PMA-C_{60} with a smaller M_n of PMA. For use in a drug delivery system, however, a smaller assembly size is

often desired. To express the enhanced permeability and retention (EPR) effect, an assembly size of 50–100 nm is desired[35]. In order to decrease the size of the assemblies to the order of a few tens of nanometers, we investigated how the ion concentration affects the association behavior by changing the salt concentration in the sample solutions.

As with the previously fabricated samples, we estimated the assembly sizes for the new samples from the time-correlation functions (Figure 4S). Most of the time-correlation functions were fitted well with a double exponential function to provide two diffusion constants, as shown in the q^2–Γ plot in **Figure 6**. Using the diffusion constant obtained from the slope of the q^2-Γ plot, we estimated the assembly size. The obtained parameters are summarized in **Table 3**. The relationship between the salt concentration and assembly size are shown in **Figure 7**. At a low salt concentration of 2.5×10^{-4} M, the assembly size is almost identical to that in pure water. However, the size became much smaller, shrinking to 20 nm with the number-based fraction higher than 99% as the salt concentration increased. A small amount of the large assembly (<1% of the number-based fraction) maintained a size between 150 nm and 200 nm in terms of their hydrodynamic diameter. In the range of 5.0×10^{-4} to 0.15 M, micelles ca. 20–30 nm in size formed. Above a concentration of 0.5 M, the solution became turbid and precipitation occurred; this is reasonably explained by the salting-out mechanism.

Theoretical and experimental studies on the weak poly-acid brush indicate that the

electric repulsion is enhanced by the small amount of salt by increasing the dissociation degree of the poly-acid[36–42]. This phenomenon is commonly understood to originate from the fact that the dissociation degree of the weak polyelectrolyte is depressed relative to the small molecular counterparts. By adding NaCl, the exchange of only H^+ and Na^+ occurs in the PMA chains serving to increase dissociation, while the intrusion of Cl^- ions is prevented by the high osmotic pressure in the crowded PMA chains. In this range, the PMA chain can be extended. However, above the critical concentration of the salt, ions derived from NaCl can enter the PMA shell and screen the electrostatic repulsion effects. This leads to the aggregation of the micelles. Considering this information, we suppose that PMA chains can form a more diffuse state in a solution with a low salt concentration than in pure water and can occupy a larger volume. This has a similar effect to that induced by increasing the M_n of PMA, as discussed in the previous section. This is consistent with the fact that smaller assemblies with 20 nm diameters are formed in the PMA-C_{60} system with a larger M_n of PMA.

Tam et al. also previously studied a nearly identical system, although they did not report the effects of the molecular weight of PMA[19,20]. They reported that PMA-C_{60} with a PMA molecular weight (M_n) of 16,000 showed the presence of a large assembly with a diameter of 90–150 nm, depending on neutralization degree at NaCl concentrations above 0.2 M[19]. This is consistent with our results, although they considered the large assembly to be composed of

micelles. The effect of salt concentration on weak polyelectrolytes is more complicated than that on strong polyelectrolytes.

Effects of Ethanol on the Large Assembly

In order to decrease the size of the aggregates by controlling other parameters besides ion concentration, we investigate how the solvent composition affects the association behavior by adding ethanol to the sample solution. In the former section, the electric interaction between the PMA chains is noted to change the assembly size. The polymer–solvent interaction may also be controlled by adding ethanol to the solution.

We examined the assembly formation at different compositions of ethanol and water. A time-correlation function was obtained by the same procedure used in the previous section (see Supporting Figure 5S), and most of the time-correlation functions were fitted well with the double exponential function. One of the exponentials is attributed to the micellar size and the other to the larger assembly. We plotted Γ against q^2, as shown in **Figure 8**. Here, the scattering vector, q, contains a refractive index, n, as $q = 4\pi n \sin\theta/\lambda$. The refractive index, which changes with the solvent composition, was estimated from the literature values (see Figure 6S and Table 6S). We confirmed that plot of Γ against q^2 shows good linearity and passes through the origin. This means that the diffusion constant obtained from the slope is the translational

diffusion constant and that the assembly shape can be assumed to be a hard sphere. We estimated the hydrodynamic diameter, D_h, by the Stokes–Einstein equation, $D = k_BT/3\pi\eta D_h$. Unlike in the former systems, the viscosity in this series is not constant at different solvent compositions. We needed to estimate the viscosity of the solvent compositions used here at 25 ºC; this was achieved by the use of literature values (see Figure 7S and Table 7S). By using the obtained value of viscosity, we estimated the assembly sizes. The assembly sizes and the number-based fractions are summarized in **Table 4**. By adding ethanol to an amount that comprises more than 25% of the solvent, the assembly size becomes much smaller, shrinking to 20 nm at a number-based fraction of nearly 100%, as shown in **Figure 9**. The assembly size is almost constant in the range of 25% to 100% ethanol.

In order to explain why ethanol induces the formation of smaller assemblies of PMA14k-C_{60}, we considered the differences between the PMA–ethanol interaction and the PMA–water interaction. Using Hansen parameters[43], we estimated the quality of the solvents in terms of their interaction with PMA. We determined ethanol to be a better solvent to PMA. In such a case, the PMA chains diffuse in ethanol and occupy a larger volume than in water. This situation would therefore produce an effect similar to that occurring in the PMA-C_{60} system with a larger M_n of PMA. This is consistent with the fact that the smaller assembly with a 20 nm diameter is formed in the PMA-C_{60} system with a larger M_n of PMA. We suppose that the

addition of ethanol can induce effects similar to those induced by increasing the molecular weight of PMA.

We have shown that the assembly size of the PMA-C_{60} system can be controlled by the molecular weight of PMA, salt concentration, and solvent composition. Particularly, the assembly size range may be divided into two groups: 20–30 nm and 150–250 nm. This non-continuous size change was also observed in the PVP-C_{60} system[26]. It suggests that a morphological change occurs between the two ranges. For example, spherical micelles may become spherical vesicles, or spherical micelles may transform into a large hierarchical assembly of micelles, as proposed by Ravi et al[11].

Our results are schematically summarized in **Figure 10**. We assume that the change in assembly size originates from the volume balance between the hydrophilic and hydrophobic parts of the system, as represented by Israelachvili's critical packing parameter[44]. Usually, the curvature made by the amphiphilic molecules affects the size and shape of the assemblies. From the DLS measurement and TEM, all assemblies in the systems examined in this study can be considered to be spherical. A larger curvature results in smaller assemblies with smaller aggregation numbers. Thus, we reasonably considered that the large assemblies (100–200 nm) would have a small curvature while the smaller assemblies would have a large curvature, as presented in **Figure 10** (a).

To show the molecular weight effect of PMA on the assembly size, we presented the difference schematically in **Figure 10** (b). Upon increase of the molecular weight, the volume of the PMA increases and the PMA exists in a cone shape rather than a rod shape. By occupying volume in a conical shape, the large curvature at the C_{60}–PMA interface would assemble in the form of a micelle. The effects of salt are summarized in **Figure 10** (c). It is well known that the addition of salt enhances the dissociation of PMA at a relatively dilute concentration of salt. Thus, a small amount of salt diffuses PMA chains by enhancing the electrostatic interactions. However, a large amount of salt can screen the electrostatic interactions, and PMA undergoes a process of salting out. The change in the PMA conformation could affect the assembly size through the difference in the PMA-C_{60} curvature, as shown in **Figure 10** (c). In terms of the addition of ethanol, PMA had a diffuse conformation in ethanol rather than in water, as displayed in **Figure 10** (d). The diffuse conformation was convenient for the formation of smaller assembly-like micelles, while a less diffuse conformation allowed the formation of larger assembly-like vesicles.

Conclusions

In this study, we synthesized PMA-C_{60} with different PMA molecular weights and investigated the assembly size formed by PMA-C_{60} in aqueous systems. We found that

PMA-C_{60} with a high molecular weight forms micelles with 20 nm diameters while PMA-C_{60} with a low molecular weight forms monodisperse assemblies with 200 nm diameters. We found that the large monodisperse assemblies transformed into micelles upon addition of ionic species or ethanol. These results provide insight into the facile control of the assembly size of fullerene-containing assemblies.

Acknowledgments

We are greatly thankful to Prof. Kohji Yoshinaga (Professor Emeritus of Kyushu Institute of Technology) for his advice in the experiments. We also thankful to Prof. Masato Yamamura (Kyushu Institute of Technology) for his kind support in the surface tension measurements, as well as to Mr. Masumi Kunisue and Mr. Noboru Wakayama for the NMR measurements and TEM observations, respectively. This work was financially supported by a grant-in-aid from JSPS (no. 19750099, 24850015).

References

(1) Prato M (1997) [60] Fullerene chemistry for materials science applications. J Mater Chem 7:1097-1109.

(2) Giacalone F, Martin N (2006) Fullerene polymers: synthesis and properties. Chem Rev 106:

5136-5190

(3) Pierini F, Lanzi M, Nakielski P, Pawlowska S, Urbanek O, Zembrzycki K, Kowalewski T A (2017) Single-material organic solar cells based on electrospun fullerene-grafted polythiophene nanofiber. Macromolecules 50:4972-4981

(4) Ren J M, Subbiah J, Zhang B, Ishitake K, Satoh K, Kamigaito M, Qiao G G, Wong E H H, Wong W W H (2016) Fullerene peapod nanoparticles as an organic semiconductor–electrode interface layer. Chem. Commun. 52:3356-3359

(5) Bosi S, Da Ross T, Spalluto G, Prato M (2003) Fullerene derivatives: an attractive tool for biological applications. European Journal of Medicinal Chemistry 38:913-923

(6) Constantin C, Neagu M, Ion R M (2010) Fullerene–porphyrin nanostructures in photodynamic therapy. Nanomedicine 5:307-317

(7) Friedman S H, DeCamp D L, Sijbesma R P, Srdanov G, Wudl F, Kenyon G L (1993) Inhibitation of the HIV-1 Protease by fullerene derivatives: model building studies and experimental verification. J. Am. Chem. Soc. 115:6506-6509

(8) Mousavi S Z, Nafisi S, Maibach H I (2017) Fullerene nanoparticle in dermatological and cosmetic applications. Nanomedicine 13:1071-1087

(9) Richardson CF, Schuster DI, Wilson SR (2000) Synthesis and characterization of water-soluble amino fullerene derivatives. Org Lett 2:1011-1014

(10) Yin P, Lin Z, Wu J, Hsu C-H, Chen X, Zhou J, Lu P, Eghtesadi S A, Yu X, Cheng S Z D, Liu T (2015) Charge-regulated spontaneous, reversible self-assembly of the carboxylic acid-functionalized hydrophilic fullerene macroanions in dilute solution. Macromolecules 48:725-731

(11) Yao Z, Tam K C (2011) Stimuli-responsive water-soluble fullerene (C_{60}) polymeric systems. Macromol Rapid Commun 32:1863-85

(12) Aroua S, Tiu EGV, Ayer M, Ishikawa T, Yamakoshi Y (2015) RAFT synthesis of poly(vinylpyrrolidone) amine and preparation of a water-soluble C_{60}-PVP conjugate. Polym Chem 6: 2616-2619

(13) J. Tam, J. Liu, Z. Yao (2013) Effect of microstructure on the antioxidant properties of fullerene polymer solutions. RSC Advance*s* 3: 4622-4627

(14) Song T, Dai S, Tam K C, Lee S Y, Goh S H (2003) Aggregation behavior of C_{60}-end-capped poly(ethylene oxide)s. Langmuir 19:4798-4803

(15) Yang J, Li L, Wang C (2003) Synthesis of a water soluble, monosubstituted C_{60} polymeric derivative and its photoconductive properties. Macromolecules 36:6060-6065

(16) Ravi R, Wang C, Dai S, Tam K C (2006) Self-assembly of well-defined mono and dual end-capped C_{60} containing polyacrylic acids in aqueous solution. Langmuir 22:7167-7174

(17) Wang C, Ravi P, Tam K C (2006) Morphological transformation of [60] fullerene-containing

poly(acrylic acid) induced by the binding of surfactant. Langmuir 22:2927-2930

(18) Wang C, Ravi P, Tam K C (2007) Supramolecular complex of [60] fullerene-grafted polyelectrolyte and surfactant: mechanism and nanostructures. Langmuir 23:8798-8805

(19) Tan C H, Ravi P, Dai S, Tam K C (2004) Polymer-induced fractal patterns of [60] fullerene containing poly(methacrylic acid) in salt solutions. Langmuir 20:9901-9904

(20) Ravi P, Dai S, Tan C H, Tam K C (2005) Self-assembly of alkali-soluble [60] fullerene containing Poly(methacrylic acid) in aqueous solution. Macromolecules 38:933-939

(21) Dai S, Ravi P, Tan C H, Tam K C (2004) Self-assembly behavior of a stimuli-responsive water-soluble [60]fullerene-containing polymer. Langmuir 20:8569-8575

(22) Yu H, Gan L H, Hu X, Gan Y Y (2007) A pH-sensitive double [60] fullerene-end-capped polymers via ATRP: Synthesis and aggregation behavior Polymer 48:2312-2321

(23) Yao Z L, Tam K C (2011) synthesis and self-assembly of stimuli-responsive Poly(2-(dimethylamino) ethyl methacrylate)-block-fullerene (PDMAEMA-b-C_{60}) and the demicellization induced by free PDMAEMA chains. Langmuir 27:6668-6673

(24) Zhou G, Harruna I I, Zhou W L, Aicher W K, Geckeler K E (2007) Nanostructured thermosensitive polymers with radical scavenging ability. Chem Euro J 13:569-573

(25) Mouri E, Moriyama M (2017) Fabrication of structure-preserving monodisperse particles of PMMA-grafted fullerenes. Fibers and Polymers 18: 2261-2268

*(26)*Mouri E, Moroi S Association behaviors of poly(*N*-vinylpyrrolidone)-grafted fullerenes in aqueous solution. *Submitted.*

(27)Wells L A, Guo H, Emili A, Sefton M V (2017) The profile of adsorbed plasma and serum proteins on methacrylic acid copolymer beads: Effect on complement activation. Biomaterials 118:74-83

(28)Okubo T (1988) Surface tension of synthetic polyelectrolyte solutions at the air-water interface. J. Colloid Int. Sci. 125:386-396

(29)Qin A, Tian M, Ramireday C, Webber S E, Munk P, Tuzar Z (1994) Polystyrene-poly(methacrylic acid) block copolymer micelles. Macromolecules 27:120-126

(30)Astafleva I, Khougaz K, Eisenberg A (1995) Micellization in block polyelectrolyte solutions. 2. fluorescence study of the critical micelle concentration as a function of soluble block length and salt concentration. Macromolecules 28:7127-7134

(31)Khougaz K, Astafieva I, Eisenberg A (1995) Micellization in block polyelectrolyte solutions. 3. Static light scattering characterization. Macromolecules 28:7135-7147

(32)Burguière C, Chassenieux C, Chaleux B (2003) Characterization of aqueous micellar solutions of amphiphilic block copolymers of poly(acrylic acid) and polystyrene prepared via ATRP. Toward the control of the number of particles in emulsion polymerization. Polymer 44:509-518

(33)Zhang L, Eisenberg A (1996) Multiple morphologies and characteristics of “crew-cut”

micelle-like aggregates of polystyrene-*b*-poly(acrylic acid) diblock copolymers in aqueous solutions. J Am Chem Soc 118:3168-3181

(34) Moffitt M, Vali H, Eisenberg A (1998) Spherical assemblies of semiconductor nanoparticles in water-soluble block copolymer aggregates. Chem Mater 10:1021-1028

(35) Meng H, Xue M, Xia T, Ji Z, Tarn D Y, Zink J I, Nel A E (2011) Use of size and a copolymer design feature to improve the biodistribution and the enhanced permeability and retention effect of doxorubicin-loaded mesoporous silica nanoparticles in a murine xenograft tumor model. ACS Nano 5:4131-4144

(36) Matějíček P, Podhájecká K, Humpolíčková J, Uhlík F, Jelínek K, Limpouchová Z, Procházka K, Špírková M (2004) Polyelectrolyte behavior of polystyrene-*block*-poly(methacrylic acid) micelles in aqueous solutions at low ionic strength. Macromolecules 37:10141-10154

(37) Israëls R, Leermakers F A M, Fleer G J (1994) On the theory of grafted weak polyacids. Macromolecules 27:3087-3093

(38) Zhulina E B, Birshtein T M, Borisov O B (1995) Theory of ionizable polymer brushes. Macromolecules 28:1491-1499

(39) Lyatskaya Y V, Leermakers F A M, Fleer G J, Zhulina E B, Birshtein T M (1995) Analytical self-consistent-field model of weak polyacid brushes. Macromolecules 28:3562-3569

(40) Currie E P K, Sieval A B, Fleer G J, Cohen-Stuart M-A (2000) Polyacrylic acid brushes: surface

pressure and salt-induced swelling. Langmuir 16:8324-8333

(41) Biesalski M, Johannsmann D, Rűhe J (2002). Synthesis and swelling behavior of a weak polyacid brush. J. Chem. Phys. 117:4988-4994

(42) Mouri E, Kaewsaiha P, Matsumoto K, Matsuoka H, Torikai N (2004) Effect of salt concentration on the nanostructure of weak polyacid brush in the amphiphilic polymer monolayer at the air/water interface. Langmuir 20:10604-10611

(43) http://polymerdatabase.com/index.html

(44) Israelachvili J N, Mitchell D J, Ninham B W (1976) Theory of self-assembly of hydrocarbon amphiphiles into micelles and bilayers. J. Chem. Soc. Faraday Trans. 72: 1525-1568

Figure Captions:

Figure 1. Surface tension variation of PMA-C_{60} aqueous solutions with PMA-C_{60} concentration.

Figure 2. Time-correlation functions for the PVP-C_{60} aqueous solutions at a scattering angle of 90º: (a) PMA2k-C_{60}, (b) PMA14k-C_{60}, (c) PMA45k-C_{60}, and (d) PMA68k-C_{60}. These time-correlation functions are fitted with exponential functions.

Figure 3. Plots of Γ vs. q^2 for the PMA-C_{60} aqueous solutions; the diffusion coefficients were evaluated from the slopes of the plots: (a) PMA2k-C_{60}, (b) PMA14k-C_{60}, (c) PMA45k-C_{60}, and (d) PMA68k-C_{60}.

Figure 4. Effect of the molecular weights of grafted PMA on the hydrodynamic diameter of the assemblies. The fractions of the smaller assemblies are also presented.

Figure 5. TEM images of the assemblies for (a) PMA14k-C_{60} and (b) PMA45k-C_{60}. Magnified images for (a) and (b) are also presented as (c) and (d), respectively.

Figure 6. Plots of Γ vs. q^2 for the PMA-C_{60} aqueous solutions with differing salt concentrations; the diffusion coefficients were evaluated from the slopes of the plots: (a) 2.5×10^{-4} M, (b) 5×10^{-4} M, (c) 2.5×10^{-3} M, (d) 5×10^{-3} M, (e) 0.05 M, and (f) 0.15 M.

Figure 7. Effect of salt concentrations on the hydrodynamic diameter of the assemblies. The fractions of the smaller assemblies are also presented.

Figure 8. Plots of Γ vs. q^2 for PMA-C_{60} in solvents with varying EtOH/water compositions; the diffusion coefficients were evaluated from the slopes of the plots: (a) 25% EtOH, (b) 55% EtOH, (c) 75% EtOH, and (d) 100% EtOH.

Figure 9. Effect of the ethanol composition in the solvents on the hydrodynamic diameter of the assemblies. The fractions of the smaller assemblies are also presented.

Figure 10. Schematics of the formation of a PMA-C_{60} micelle and a large assembly with small and large curvatures (a), along with three parameters: (b) molecular weights, (c) salt concentration, and (d) EtOH compositions.

Table 1. Characteristics of P*t*BMA.

Sample Code	M_n *	M_w/M_n **
P*t*BMA3k	3,200	1.57
P*t*BMA23k	23,000	1.48
P*t*BMA74k	74,000	1.49
P*t*BMA113k	113,000	1.61

**Estimated by GPC measurement in THF with PEG standards.

Table 2. Hydrodynamic diameters of PMA-C_{60} assemblies in water.

Sample Code	D_{h1} / nm	D_{h2} / nm (number fraction, %)
PMA2k-C_{60}	-	321 (100)
PMA14k-C_{60}	-	189 (100)
PMA45k-C_{60}	22 (99.97)	123 (0.03)
PMA65k-C_{60}	20 (ca.100)	172 (~ 0)

The values in parenthesis are the number-based fraction (%) based on Maquardt analysis of data measured at 90º.

Table 3. Hydrodynamic diameters of PMA14k-C_{60} assemblies in NaCl aqueous solutions.

NaCl concentration / M	D_{h1} / nm (number fraction, %)	D_{h2} / nm (number fraction, %)
0	-	189 (100)
2.5×10^{-4}	-	185 (100)
5.0×10^{-4}	27 (99.93)	153 (0.07)
2.5×10^{-3}	29 (99.96)	170 (0.04)
5.0×10^{-3}	30 (ca. 100)	156 (~0)
0.05	25 (99.97)	198 (0.03)
0.15	34 (99.63)	183 (0.37)
0.5	aggregated	

The values in parenthesis are the number-based fraction (%) based on Maquardt analysis of data measured at 90º.

Table 4. Characteristics of PMA14k-C_{60} in water-ethanol mix solvent.

Ethanol fraction / %	D_{h1} / nm (number fraction, %)	D_{h2} / nm (number fraction, %)
0	-	189 (100)
25	21(99.85)	114 (0.15)
50	18 (99.59)	149 (0.41)
75	18 (97.08)	235 (2.92)
100	32 (99.12)	234 (0.88)

The values in parenthesis are the number-based fraction (%) based on Maquardt analysis of data measured at 90º.

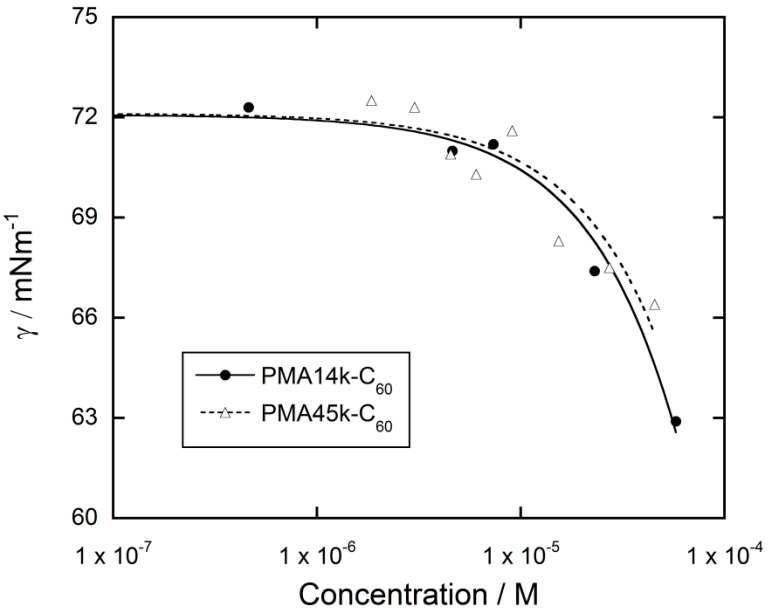
75
72
69
66
63
60
γ / mNm-1
PMA14k-C60
PMA45k-C60
1 x 10-7
1 x 10-6
1 x 10-5
1 x 10-4
Concentration / M

Fig.1

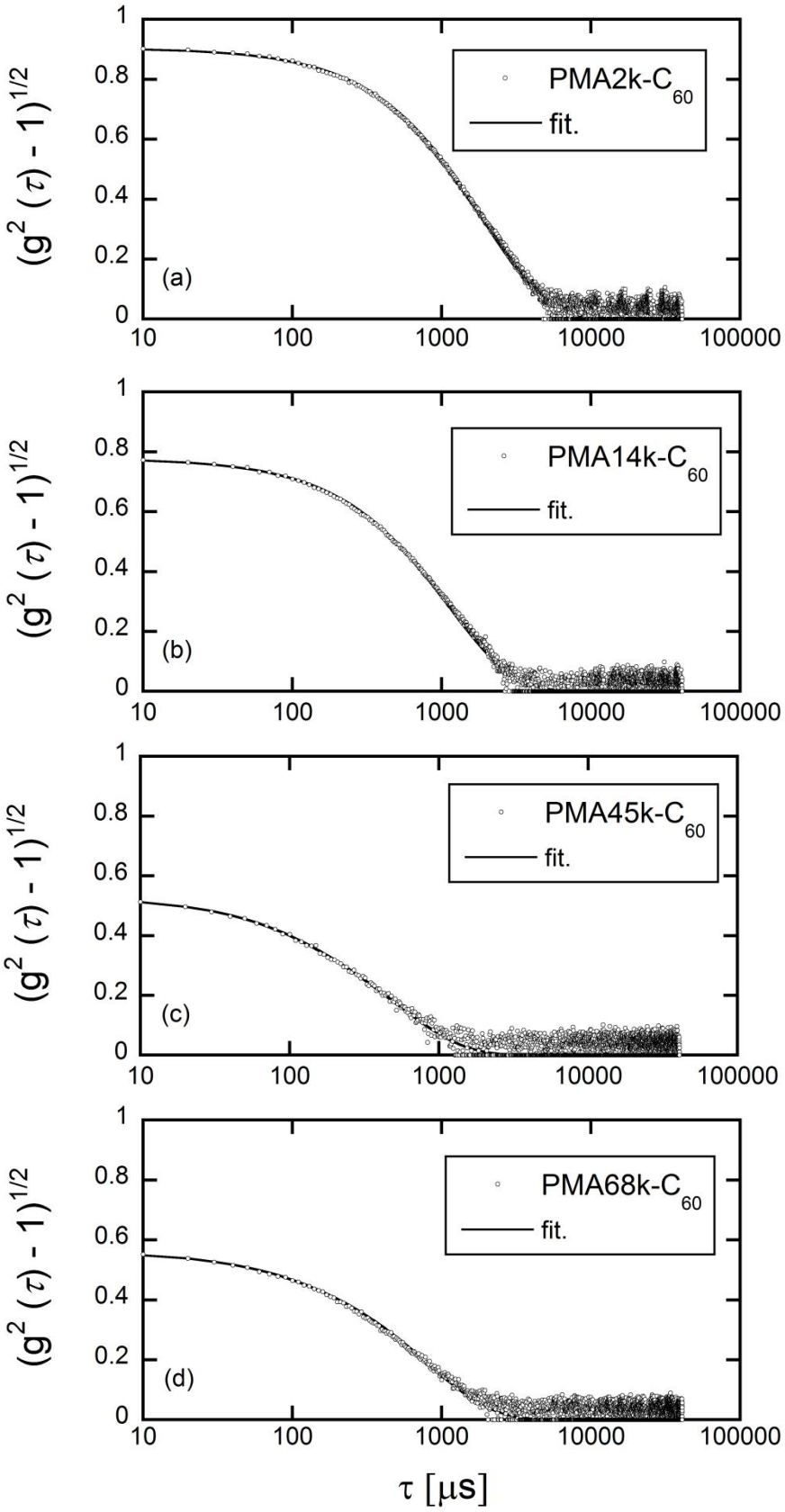
(g2 (τ) - 1)1/2
PMA2k-C60
fit.
(a)
PMA14k-C60
fit.
(b)
PMA45k-C60
fit.
(c)
PMA68k-C60
fit.
(d)
0
0.2
0.4
0.6
0.8
1
10
100
1000
10000
100000
τ [μs]

Fig.2

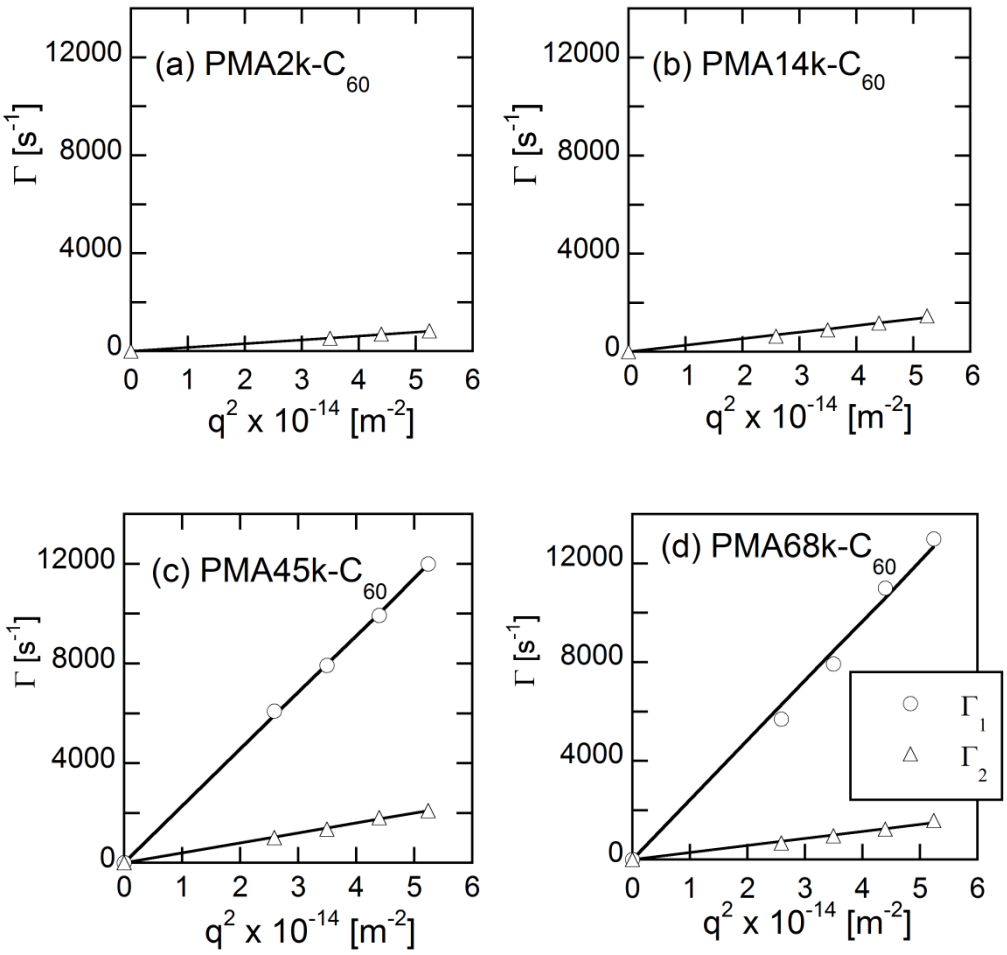
(a) PMA2k-C60
(b) PMA14k-C60
(c) PMA45k-C60
(d) PMA68k-C60
Γ [s-1]
q2 x 10-14 [m-2]
Γ1
Γ2

Fig.3

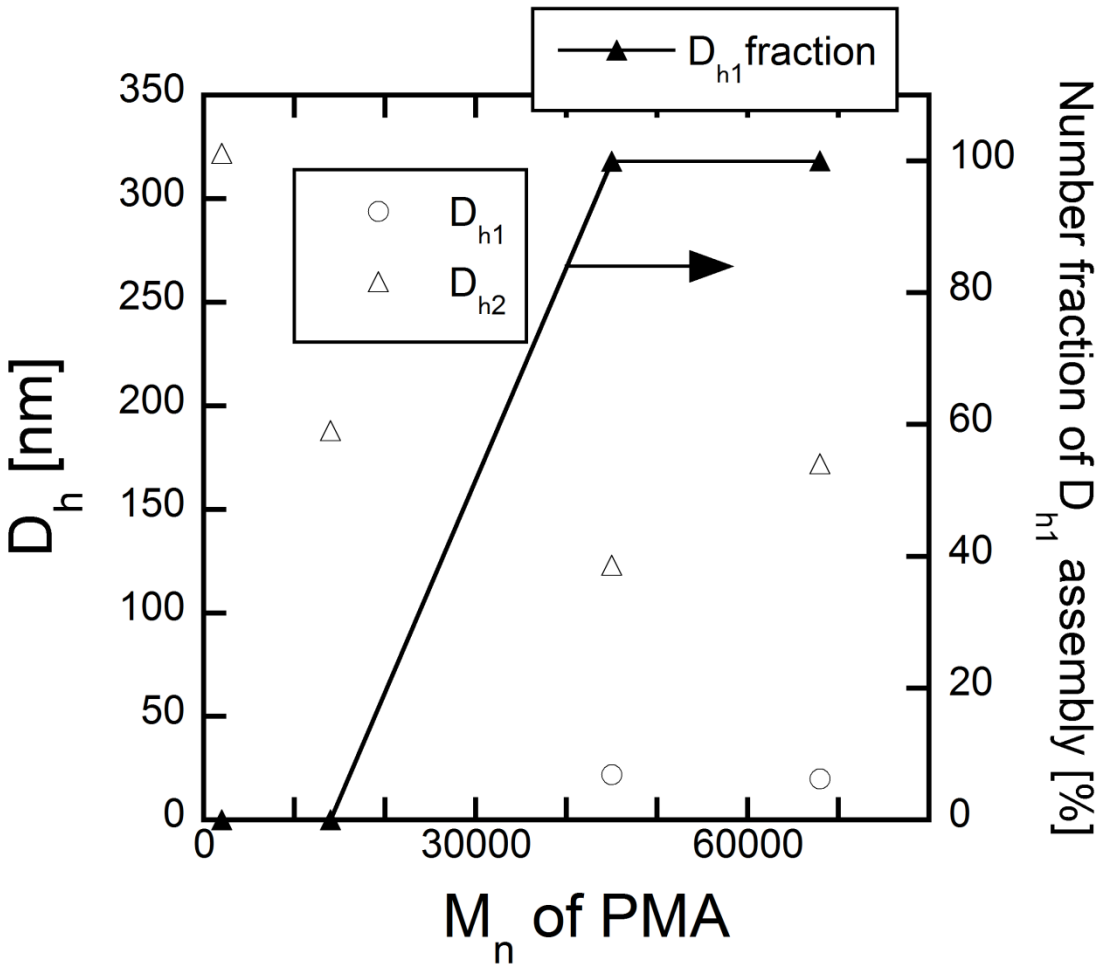
D_h1 fraction
D_h1
D_h2
D_h [nm]
Number fraction of D_h1 assembly [%]
M_n of PMA
0
50
100
150
200
250
300
350
0
20
40
60
80
100
0
30000
60000

Fig.4

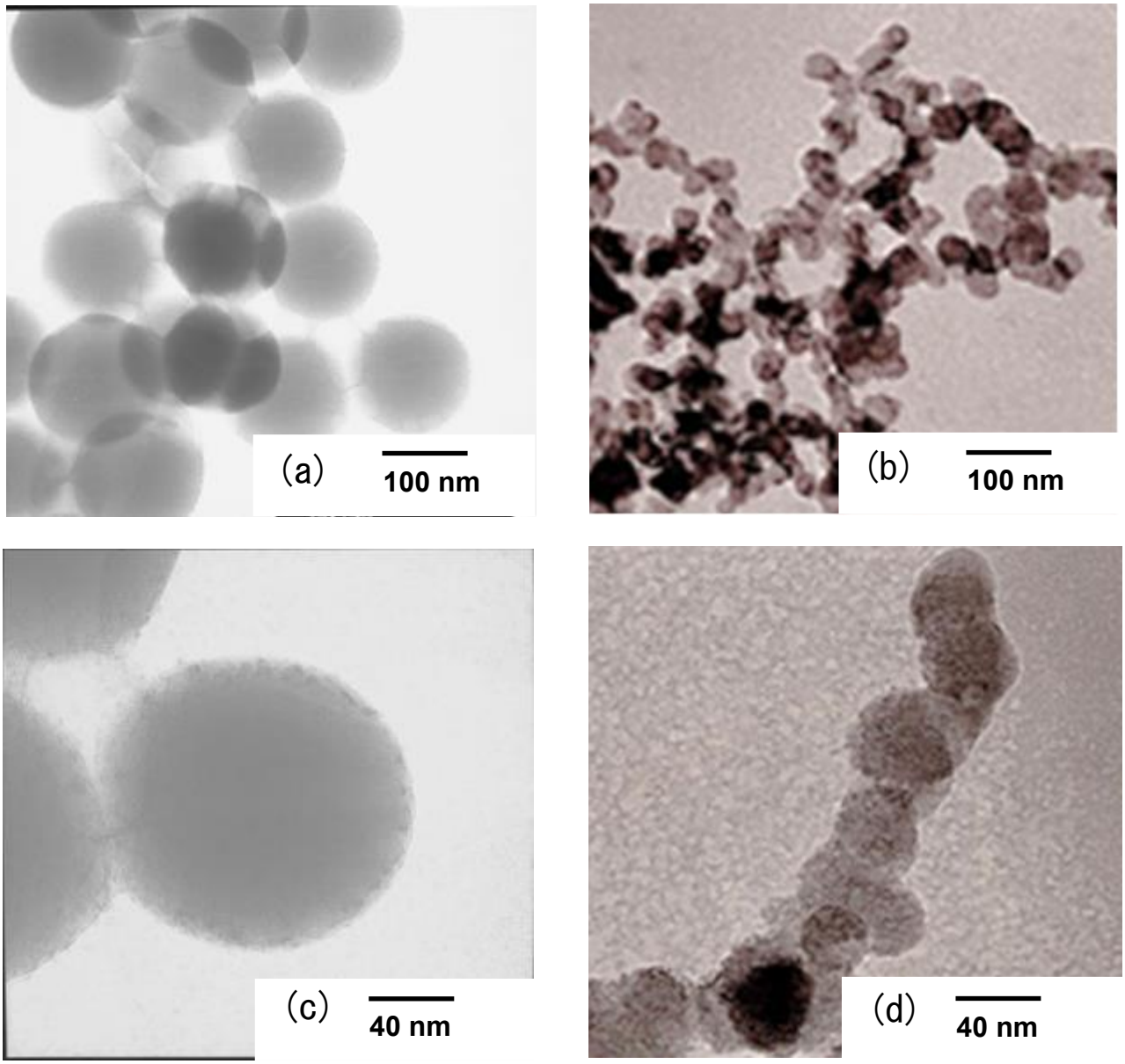

Fig.5

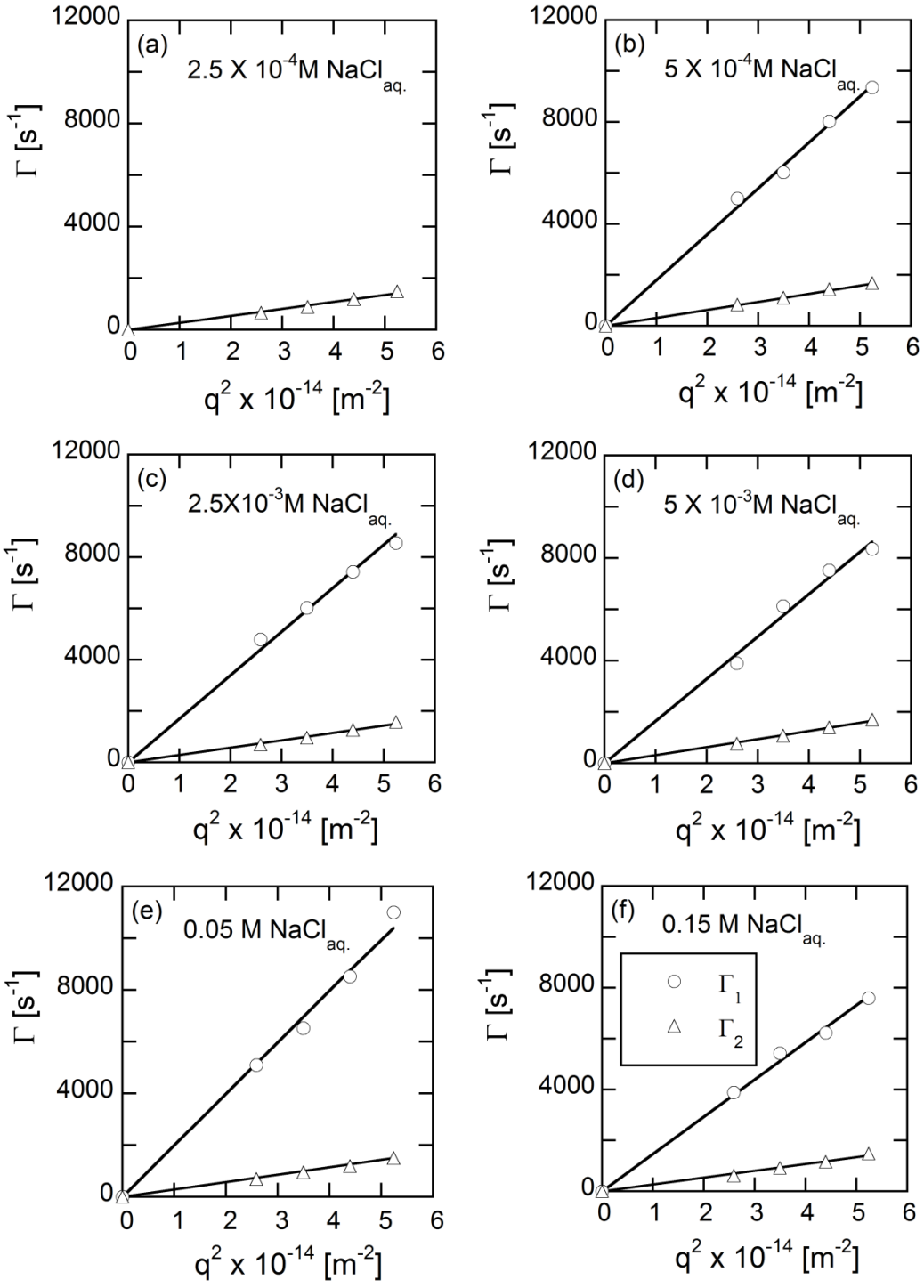
(a)
2.5 X 10-4M NaCl aq.
(b)
5 X 10-4M NaCl aq.
(c)
2.5X10-3M NaCl aq.
(d)
5 X 10-3M NaCl aq.
(e)
0.05 M NaCl aq.
(f)
0.15 M NaCl aq.
Γ1
Γ2
Γ [s-1]
q2 x 10-14 [m-2]
0
4000
8000
12000
0 1 2 3 4 5 6

Fig.6

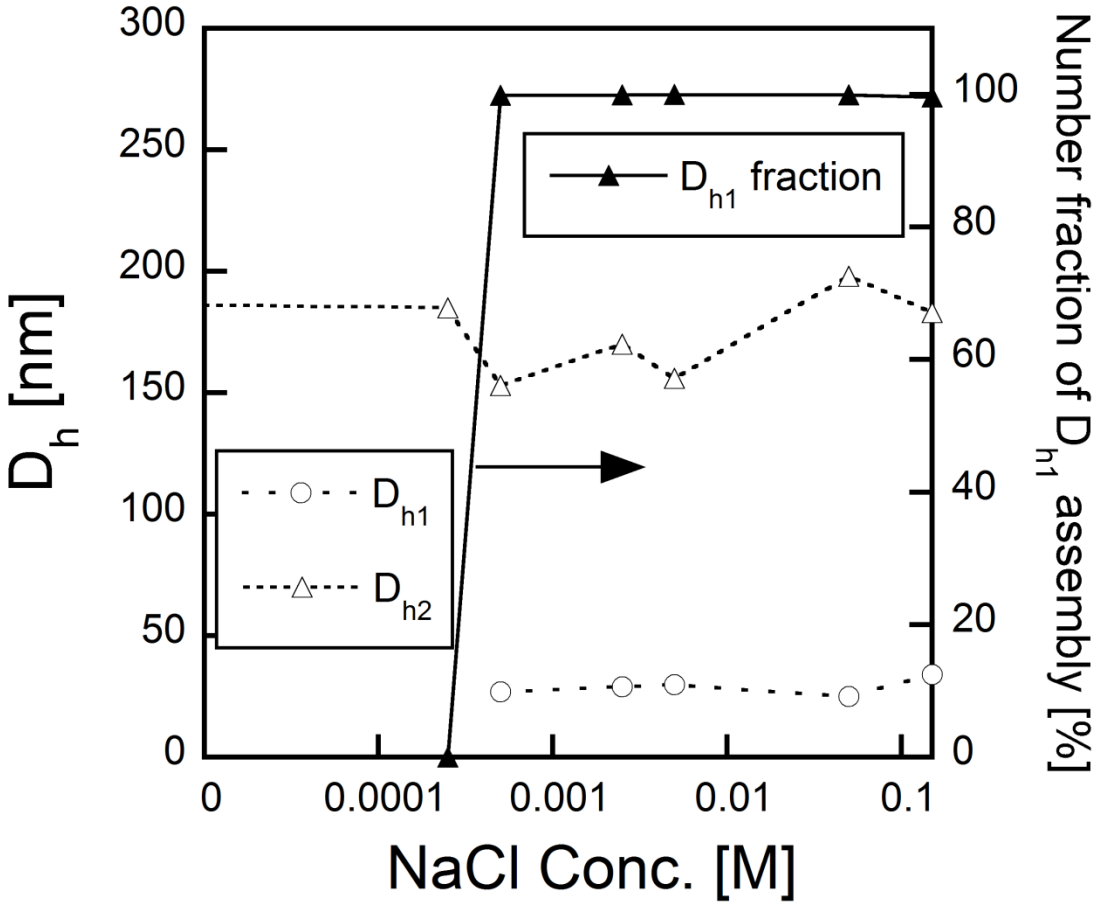
300
250
200
150
100
50
0
D_h [nm]
100
80
60
40
20
0
Number fraction of D_h1 assembly [%]
D_h1 fraction
D_h1
D_h2
0
0.0001
0.001
0.01
0.1
NaCl Conc. [M]

Fig.7

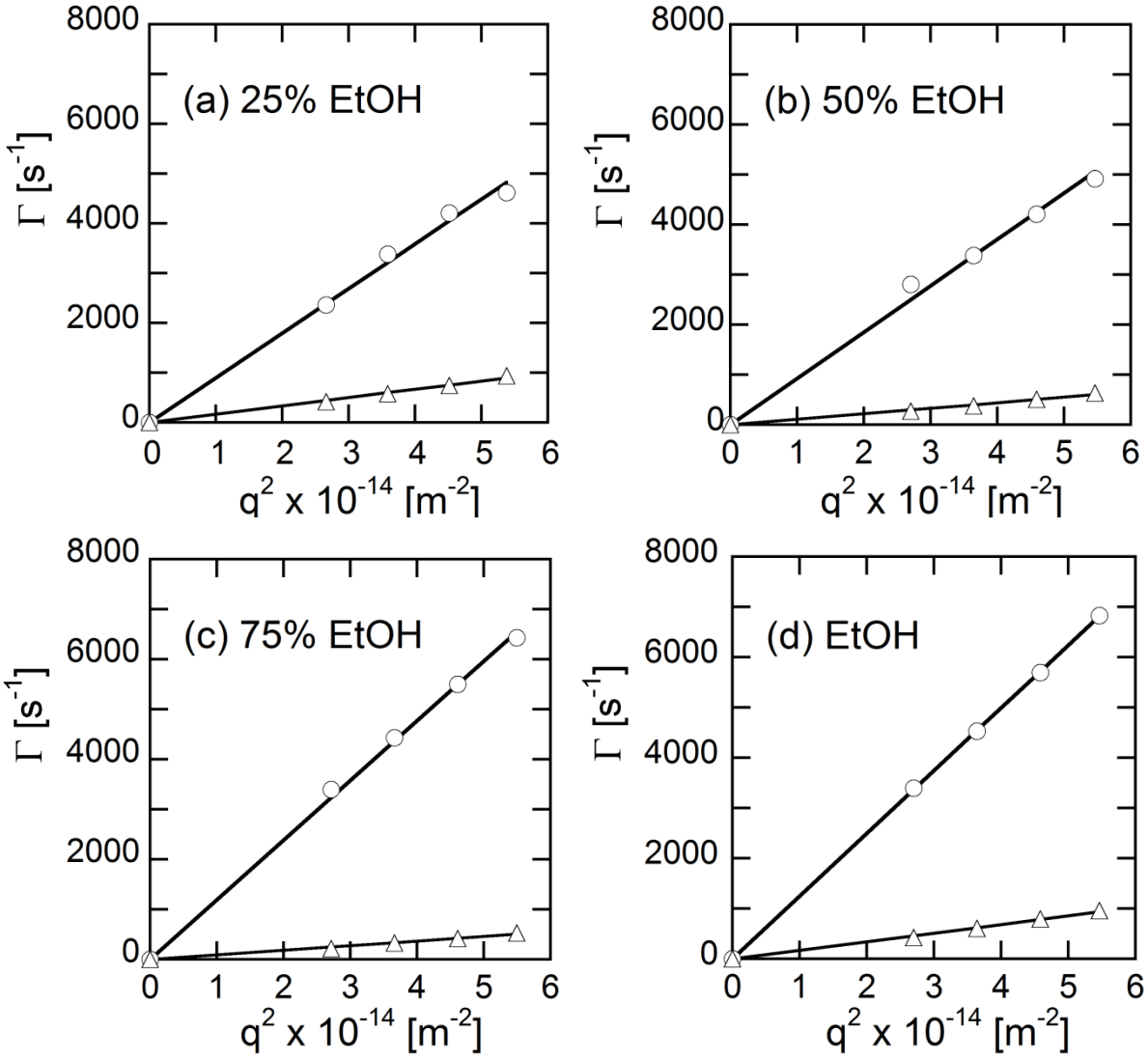
(a) 25% EtOH
(b) 50% EtOH
(c) 75% EtOH
(d) EtOH
Γ [s-1]
q2 x 10-14 [m-2]
0
2000
4000
6000
8000
0
1
2
3
4
5
6

Fig.8

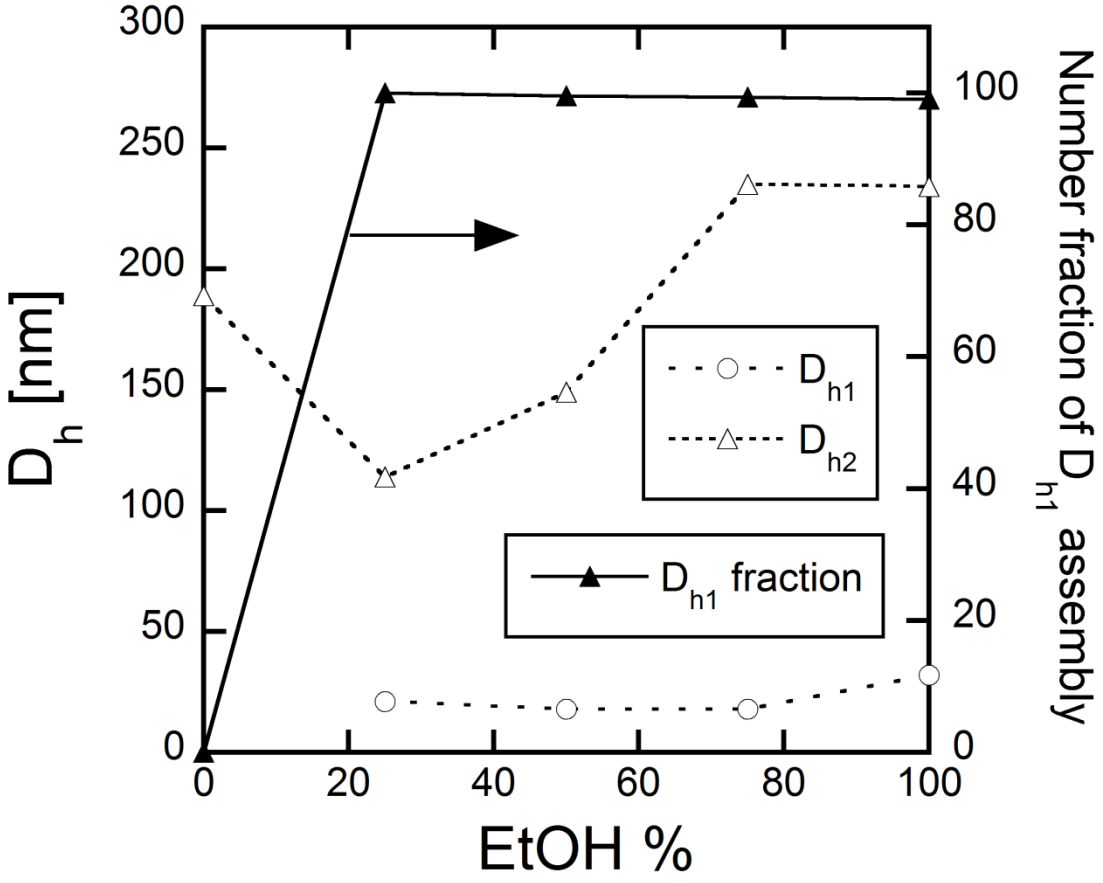
300
250
200
150
100
50
0
D_h [nm]
0
20
40
60
80
100
EtOH %
100
80
60
40
20
0
Number fraction of D_h1 assembly
D_h1
D_h2
D_h1 fraction

Fig.9

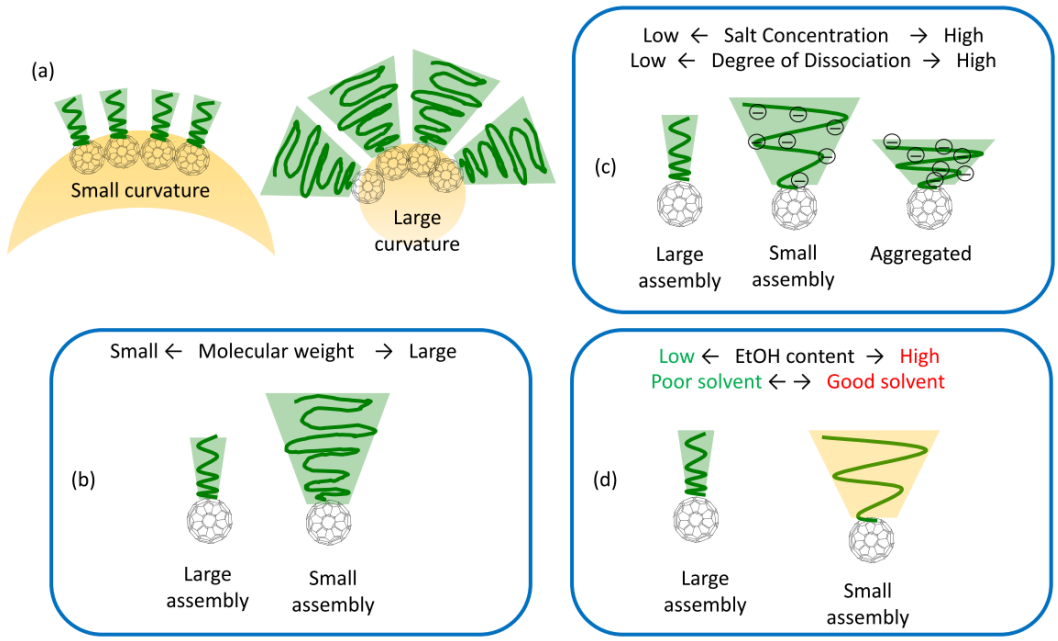
(a)
Small curvature
Large curvature
(b)
Small ← Molecular weight → Large
Large assembly
Small assembly
(c)
Low ← Salt Concentration → High
Low ← Degree of Dissociation → High
Large assembly
Small assembly
Aggregated
(d)
Low ← EtOH content → High
Poor solvent ← → Good solvent
Large assembly
Small assembly

Fig.10

Control of Assembly Size of Poly (Methacrylic Acid)-*grafted* Fullerenes in Aqueous Solution

Supporting Information

Emiko Mouri, Sanami Moroi

Department of Applied Chemistry, Faculty of Engineering, Kyushu Institute of Technology,
1-1 Sensui, Tobata, Kitakyushu, Fukuoka 804-8550, Japan

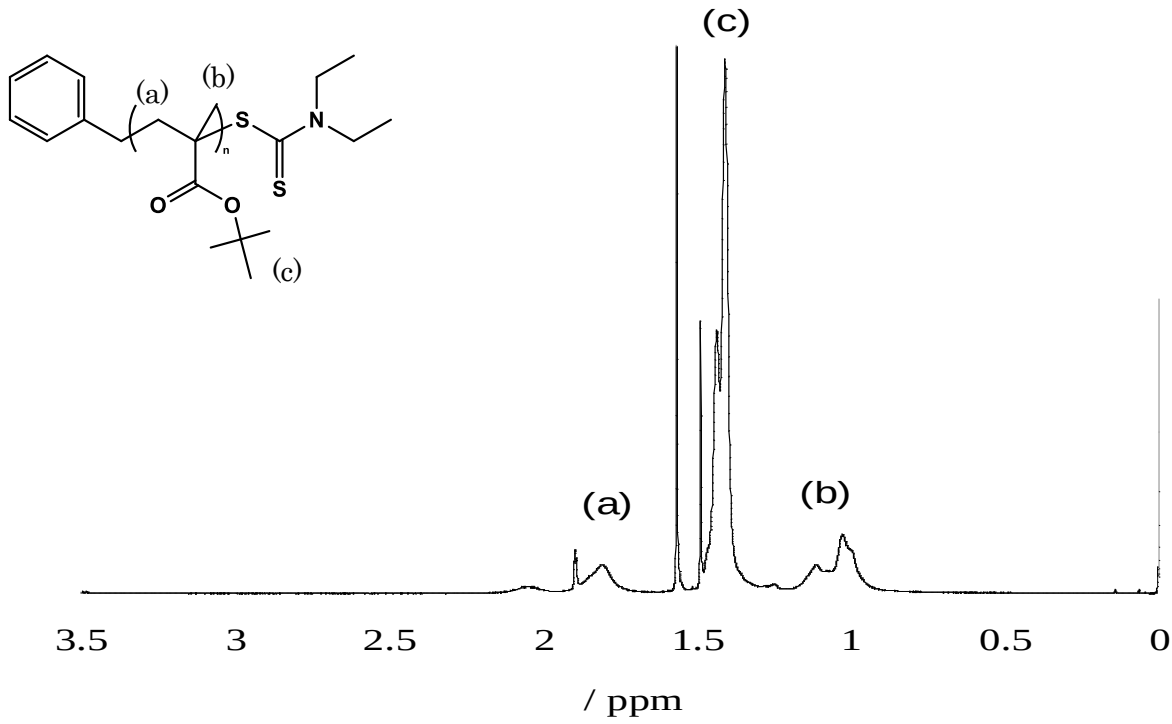

Figure 1S. [1]H-NMR spectrum of poly(*tert*-butyl methacrylate).

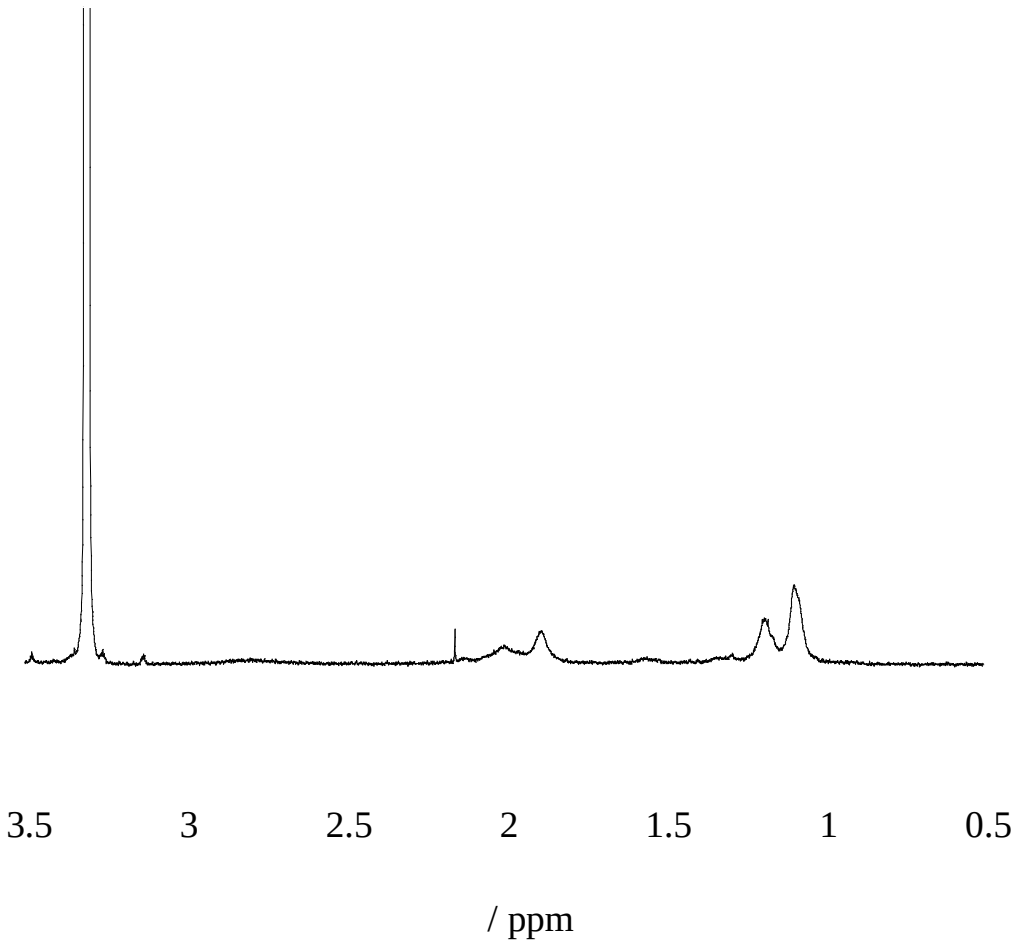

Figure 2S. ^{1}H-NMR spectrum of PMA-C_{60}. (solvent: MeOH-d_4)

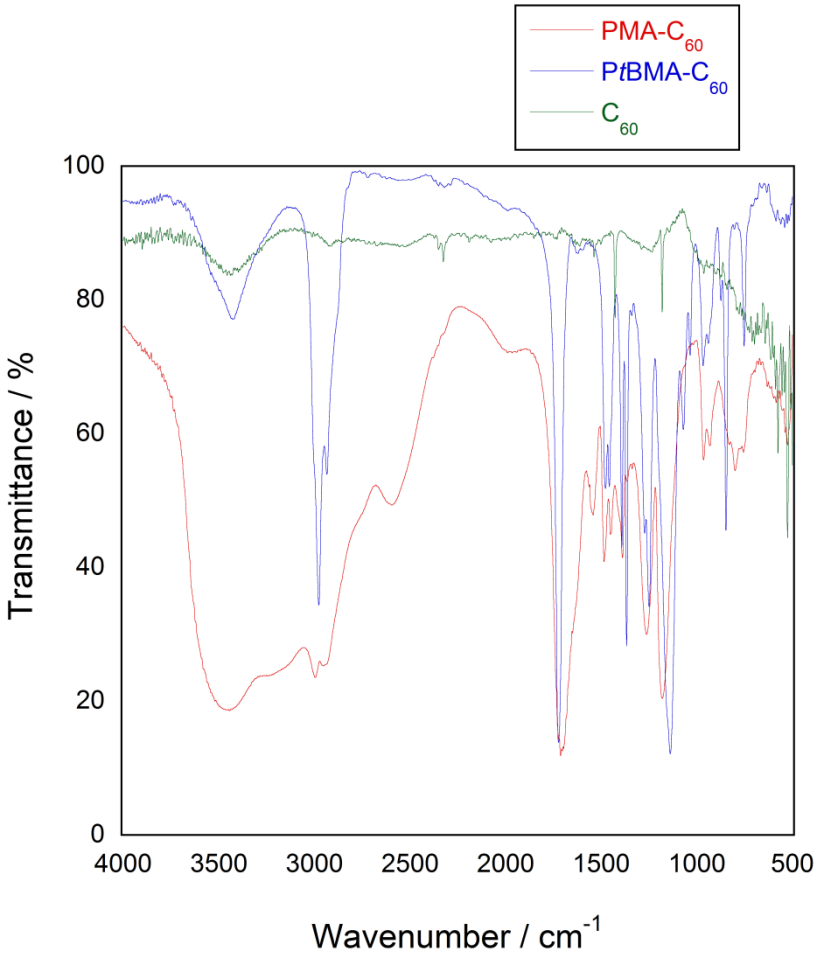

Figure 3S. IR spectra of C_{60}, P*t*BMA-C_{60} and PMA-C_{60}.

Table 1S. Synthetic feeds and irradiation condition in P*t*BMA polymerization.

Sample code	*t*BMA/ ml	BDDC / mg	1,4-dioxane / ml	Irradiation time / h
P*t*BMA3k	3	105	3	4
P*t*BMA23k	3	28.0	3	5
P*t*BMA74k	3	4.4	3	3
P*t*BMA113k	3	2.2	-	3

Table 2S. Synthetic feeds and irradiation condition in P*t*BMA-C_{60} preparation.

Sample code	P*t*BMA / mg	C_{60} / mg	dichlorobenzene / ml	Irradiation time / h
P*t*BMA3k-C_{60}	100	72	8	12
P*t*BMA23k-C_{60}	100	9.4	8	12
P*t*BMA74k-C_{60}	200	5.8	8	12
P*t*BMA113k-C_{60}	200	4.3	8	12

Table 3S. Hydrodynamic diameters of PMA-C_{60} assemblies in water.

Sample Code	D_{h1} / nm	D_{h2} / nm (number fraction, %)
PMA2k-C_{60}	-	156±37
PMA14k-C_{60}	-	119±29
PMA45k-C_{60}	20 ±3	94±21
PMA65k-C_{60}	26 ±3	117±29

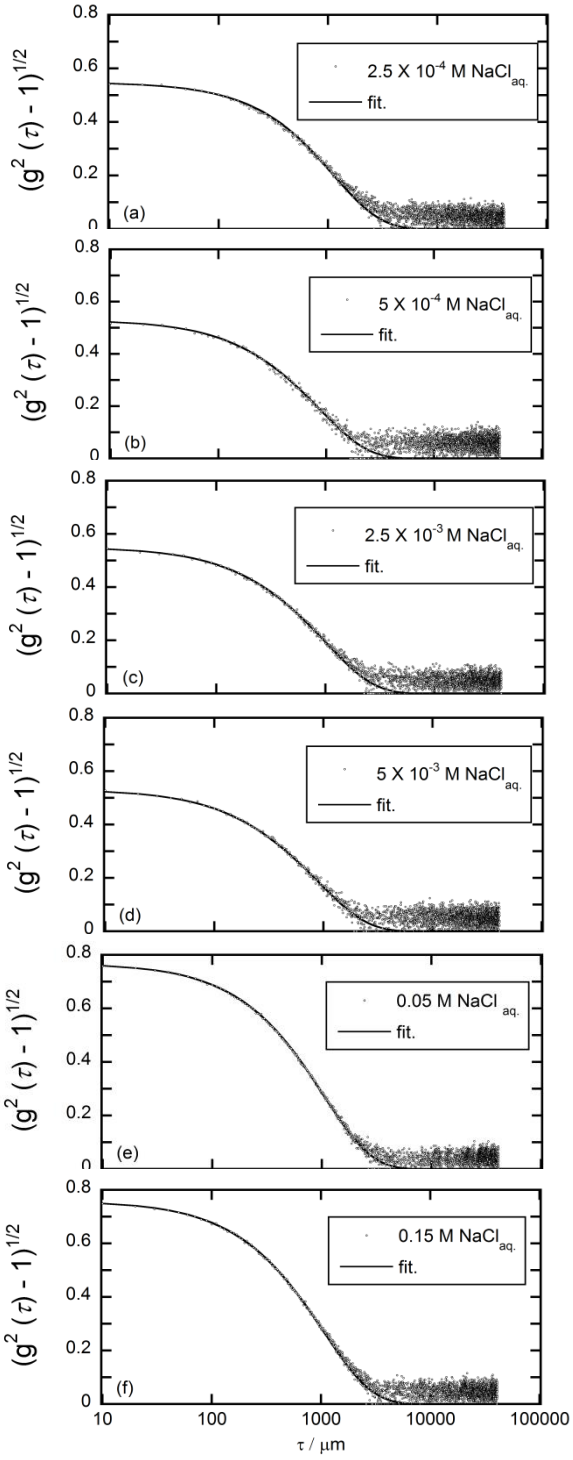

Figure 4S. Time correlation function for the PMA14k-C_{60} in aqueous solutions with different salt concentrations; (a) 2.5 X 10^{-4} M, (b) 5.0 X 10^{-4} M, (c) 2.5 X 10^{-3} M, (d) 5.0 X 10^{-3} M, (e) 0.05 M, and (f) 0.15 M. These time-correlation functions are fitted with exponential functions.

Table 4S. Hydrodynamic diameters of PMA14k-C_{60} assemblies in NaCl aqueous solutions.

NaCl concentration / M	D_{h1} / nm	D_{h2} / nm
0	-	119±29
2.5 x 10^{-4}	-	93±20
5.0 x 10^{-4}	20±2	114±24
2.5 x 10^{-3}	12±1	89±20
5.0 x 10^{-3}	4±4	-
0.05	19±2	86±21
0.15	20±2	146±29
0.5	aggregated	

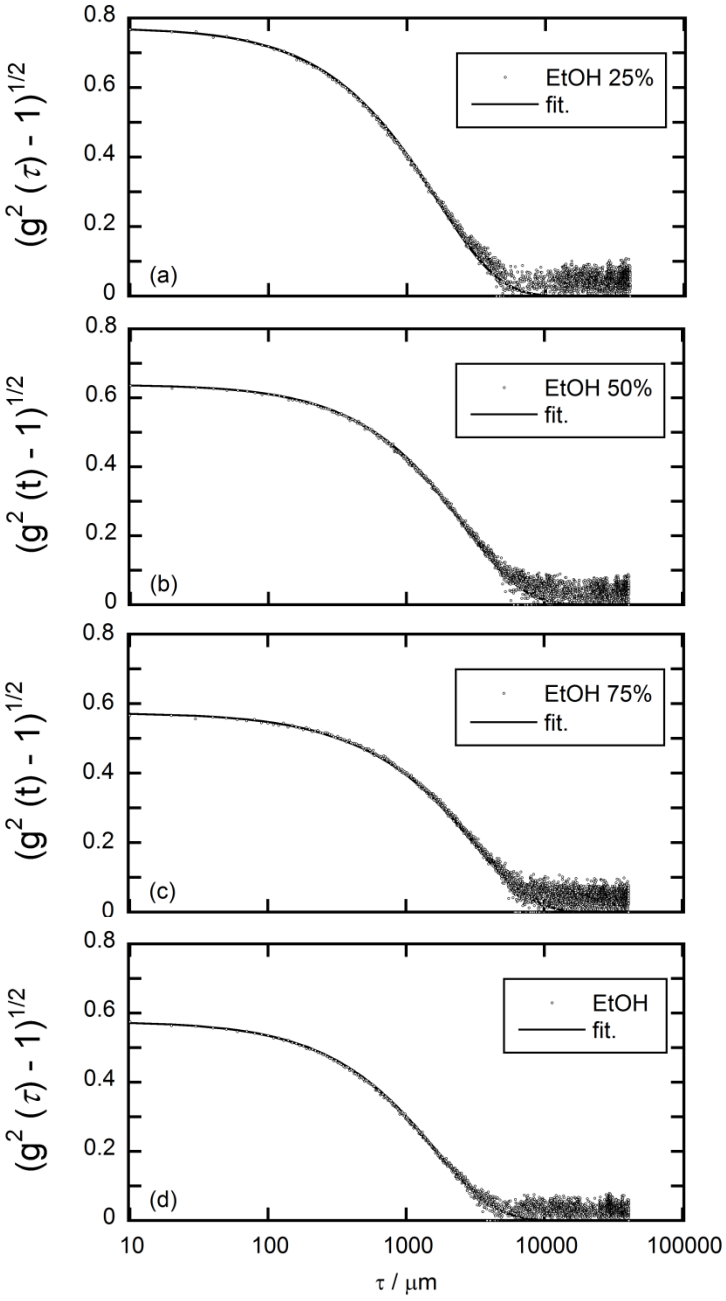

Figure 5S. Time correlation function for the PMA14k-C_{60} in ethanol-water binary solvent at a scattering angle of 90º: (a) EtOH 25%, (b) EtOH 50%, (c) EtOH 75%, and (d) EtOH 100%. These time-correlation functions are fitted with exponential functions.

Table 5S. Characteristics of PMA14k-C_{60} in water-ethanol mix solvent.

Ethanol fraction /%	D_{h1} / nm	D_{h2} / nm
0	-	119±29
25	18±2	78±18
50	24±3	106±24
75	48±3	333±69
100	32±4	163±38

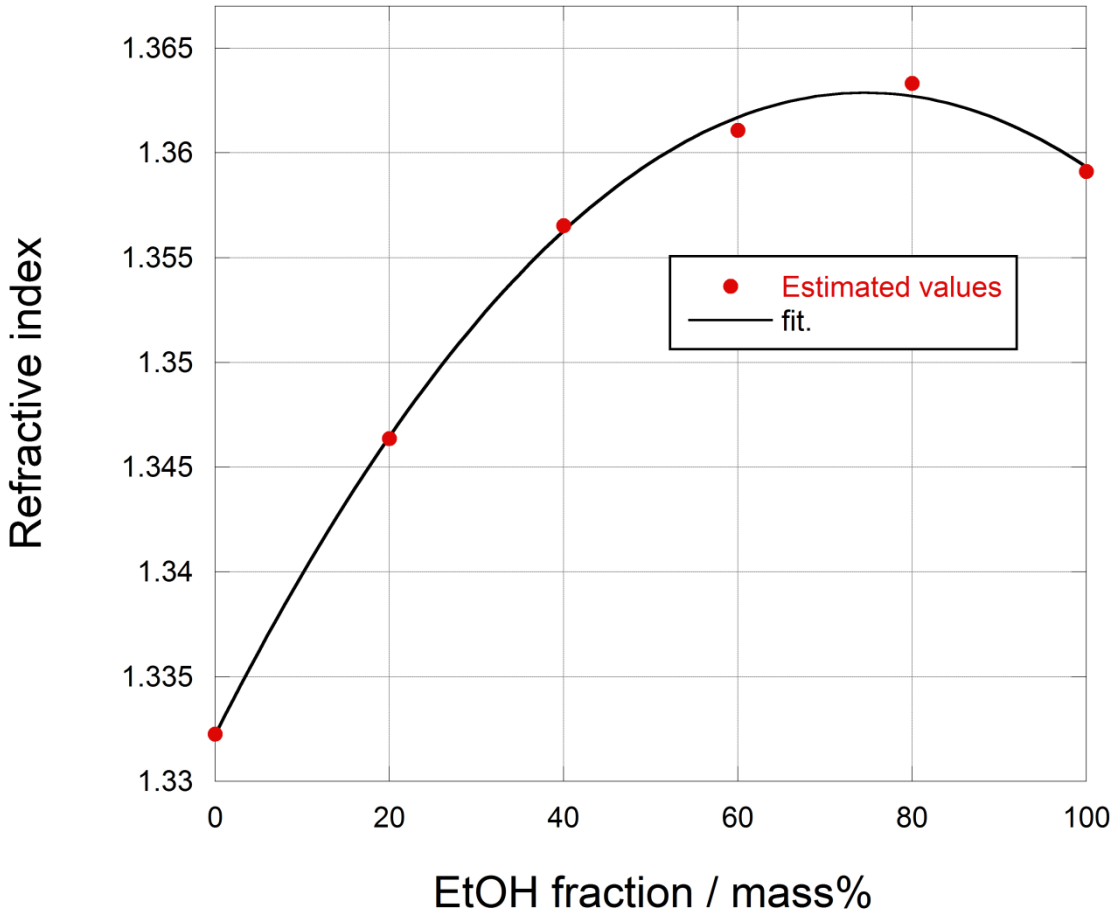

Figure 6S. Estimation of refractive indexes for ethanol-water binary solvents. By using the data for 15 and 30°C in the literature, we estimate the temperature dependence of refractive indexes at each binary solution. The plot shows calculated refractive indexes at 25 °C .

Reference: Handbook of Chemistry: Pure Chemistry, 5th ed. The Chemical Society of Japan, 2004 Maruzen publishing, Tokyo.

Table 6S. Refractive indexes of ethanol-water binary solvents.

Ethanol / mass%	Refractive index
0	1.3329
25	1.3493
50	1.3595
75	1.3629
100	1.3594

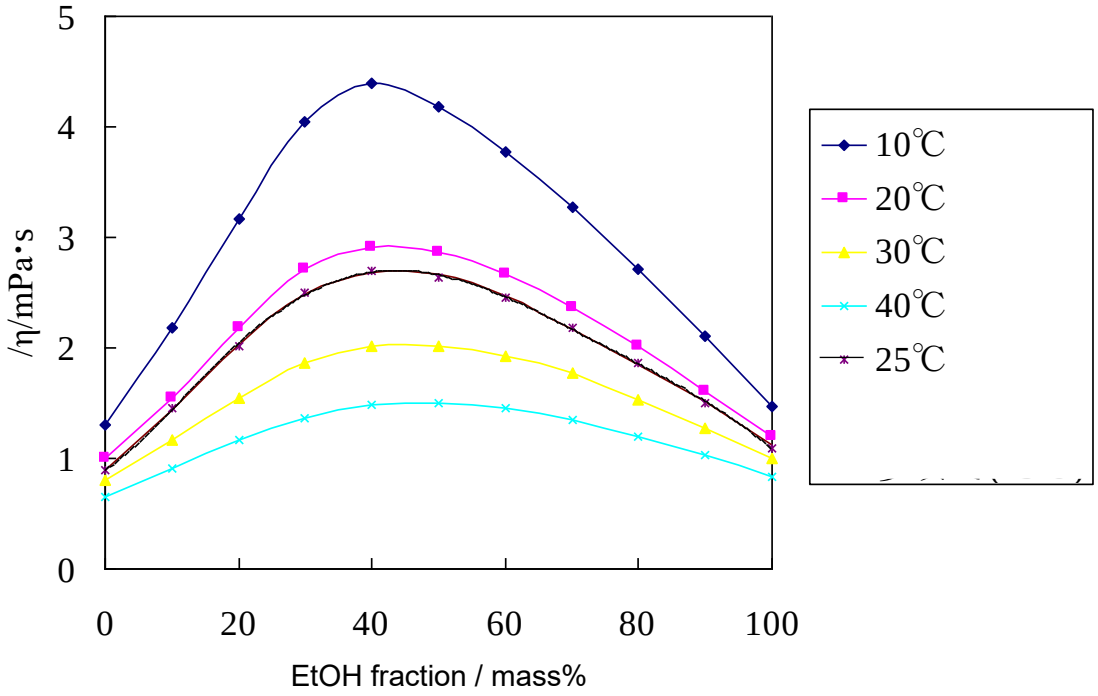

Figure 7S. Estimation of viscosities of ethanol-water binary solvents. The data for 10, 20, 30, and 40 degree is the literature values. By estimating the temperature dependence of viscosity at each binary solution, we obtained the viscosities at 25 ℃ .

Reference: Handbook of Chemistry: Pure Chemistry, 5th ed. The Chemical Society of Japan, 2004 Maruzen publishing, Tokyo.

Table 7S. Estimated viscosity at 25 ℃ for EtOH-water binary system used in the DLS analysis.

Ethanol / vol%	Viscosity / mPa・s
0	0.8902
25	2.285
50	2.643
75	2.014
100	1.084